

Kac's isospectrality question revisited in neutrino billiards

Pei Yu,¹ Barbara Dietz^{1,*}, Hong-Ya Xu,² Lei Ying², Liang Huang,^{1,†} and Ying-Cheng Lai^{2,3}
¹*School of Physical Science and Technology, and Key Laboratory for Magnetism and Magnetic Materials of MOE, Lanzhou University, Lanzhou, Gansu 730000, China*
²*School of Electrical, Computer and Energy Engineering, Arizona State University, Tempe, Arizona 85287, USA*
³*Department of Physics, Arizona State University, Tempe, Arizona 85287, USA*



(Received 24 September 2019; accepted 9 March 2020; published 27 March 2020)

“Can one hear the shape of a drum?” Kac raised this famous question in 1966, referring to the possibility of the existence of nonisometric planar domains with identical Dirichlet eigenvalue spectra of the Laplacian. Pairs of nonisometric isospectral billiards were eventually found by employing the transplantation method which was deduced from Sunada's theorem. Our main focus is the question to what extent isospectrality of nonrelativistic quantum billiards is present in the corresponding relativistic case, i.e., for massless spin-1/2 particles governed by the Dirac equation and confined to a domain of corresponding shape by imposing boundary conditions on the wave function components. We consider those for neutrino billiards [Berry and Mondragon, *Proc. R. Soc. London A* **412**, 53 (1987)] and demonstrate that the transplantation method fails and thus isospectrality is lost when changing from the nonrelativistic to the relativistic case. To confirm this we compute the eigenvalues of pairs of neutrino billiards with the shapes of various billiards which are known to be isospectral in the nonrelativistic limit. Furthermore, we investigate their spectral properties, in particular, to find out whether not only their eigenvalues but also the fluctuations in their spectra and their length spectra differ.

DOI: [10.1103/PhysRevE.101.032215](https://doi.org/10.1103/PhysRevE.101.032215)**I. INTRODUCTION**

The question of Kac [1] can be reformulated as follows: “Can the resonance frequency spectra of two or even more nonisometric drums be identical, that is, isospectral?”; see [2] for a detailed overview. The normal modes U of a drum consisting of a rigid frame and a membrane fixed to it are obtained by solving the two-dimensional wave equation $(\frac{1}{2}\Delta + \omega^2)U(\vec{\rho} \in \Omega) = 0$ for the membrane with the Dirichlet boundary condition $U(\vec{\rho} \in \partial\Omega) = 0$, where Ω denotes the membrane domain and $\partial\Omega$ the boundary, i.e., the frame of the drum. Kac's question is of particular relevance in the context of the inverse problem, i.e., the unambiguous characterization of a system based on the exclusive knowledge of its eigenvalue spectrum. Accordingly it triggered numerous intensive investigations in systems described by a wave equation which is mathematically identical to the one given above like, for example, the two-dimensional Helmholtz equation or the Schrödinger equation [3,4] for nonrelativistic quantum billiards (QBs). Furthermore, the studies were extended to bounded systems governed by such a wave equation with Neumann boundary conditions requiring the vanishing of the normal derivative $\partial_n U(\vec{\rho} \in \partial\Omega)$, and with mixed Dirichlet and Neumann boundary conditions [5,6]. In Refs. [7,8] necessary conditions were provided to be fulfilled by nonisometric billiards in order to be isospectral. After Kac posed his question numerous examples of isospectral higher-dimensional Riemannian manifolds were constructed

[2]. However, Kac's original question refers to isospectrality of planar domains. Based on Sunada's procedure for finding isospectral manifolds [9], Gordon, Webb, and Wolpert [10] succeeded only in 1992 in constructing nonisometric two-dimensional billiards with identical eigenvalue spectra and thus to give a negative answer to Kac's question. Using the method of *transplantation* of wave functions [11] they proved both Dirichlet and Neumann isospectrality of the renowned pair of billiards [12] shown in Fig. 1. One year later isospectrality was demonstrated for these billiards experimentally in flat microwave resonators of corresponding shape [13] for the first 54 eigenvalues. Generally, the nonisometric pairs of Dirichlet and Neumann isospectral domains constructed in the Euclidian plane are all nonconvex. Convex ones were designed in the hyperbolic plane, again by employing the transplantation method [14]. The essential ideas of the transplantation method are to compose the billiards by gluing together several copies of a base structure at straight parts of its boundary and to generate the wave functions of one billiard in terms of superpositions of translations of the wave functions in the interior of these building blocks. Here, the only requirement on the building block is that its boundary possesses three noncollinear straight-edge parts thus allowing the design of more involved geometries [15] than those shown in Fig. 1. Chapman [15] proposed a simple procedure for the construction of pairs of Neumann or Dirichlet isospectral billiards, namely the *paper-folding* method.

Buser [16] constructed nonisometric and isospectral billiards by using equilateral, right-angle, or acute-angle triangles as building blocks. In Ref. [17] isospectral billiards with a chaotic classical dynamics were realized by gluing together copies of a right-angle triangular building block

*dietz@lzu.edu.cn

†huangl@lzu.edu.cn

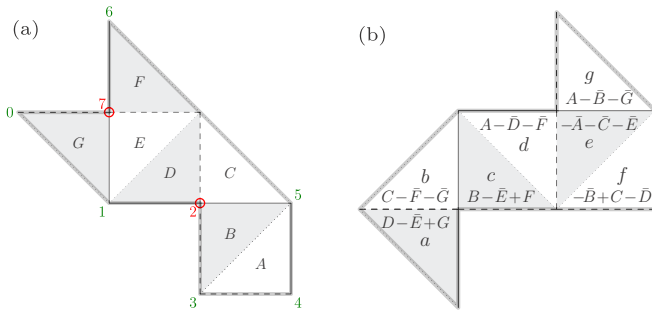


FIG. 1. Well-known pair of plane nonisometric, isospectral billiards [10], where Dirichlet conditions are assumed along the boundary. Domain 1 shown in (a) is constructed by successive reflections of the triangular building block A at respectively one of its three edges plotted as dashed, dotted, and solid lines. The numbers mark the corners. Domain 2 shown in (b) is obtained from (a) by applying the transplantation method as indicated in the building blocks $T = a, b, \dots, g$, which yields its wave functions through a superposition of translations of those in the interior of the building blocks $T = A, B, \dots, G$ of domain 1. In some cases the latter need to be translated and reflected at one of their edges so that they are on top of the respective new building block and are accordingly denoted by \bar{T} [2,15].

with a circular hole and Dirichlet boundary conditions at the walls, and were investigated numerically and experimentally with flat microwave resonators. Similarly, isospectral billiards with a piecewise fractal boundary were achieved with a suitable choice of the building block [18]. In Refs. [19,20] the exterior Neumann scattering problem was analyzed in addition to the interior Dirichlet eigenvalue problem, and it was demonstrated that nonisometric isospectral billiards may be distinguished by measuring cross sections resulting from wave scattering off the boundary of the domains from the exterior. Yet, isoscattering quantum graphs can be realized based on the isospectral construction method developed in [21,22] by appropriately attaching leads either to isospectral graphs [23] or to certain open graphs [24,25]. This has been verified experimentally with microwave networks [26].

In the present article we consider nonisometric pairs of two-dimensional domains corresponding to isospectral QBs and address the following question: will the eigenvalue spectra still be identical if we replace the nonrelativistic Schrödinger equation with Dirichlet boundary conditions by the Dirac equation of a massless spin-1/2 particle confined to either of these domains? This question is of relevance in the field of relativistic quantum chaos which emerged recently [27–38] with the pioneering fabrication of graphene [39–41]; see also Refs. [42–44] for recent reviews. To obtain an answer, we analyzed neutrino billiards (NBs) of corresponding shapes which were introduced in the seminal work of Ref. [45] and given that name, even though they refer to *massless* spin-1/2 particles confined to a bounded planar domain. We came to the result that the eigenvalues of pairs of NBs with shapes shown in Fig. 1 and, in general, of pairs of nonisometric isospectral QBs do not coincide. We attribute this to the failure of the transplantation method, which has been used to construct all isospectral QBs, for NBs.

In order to get insight into the similarities and differences of the properties of NBs with such shapes in the ray-dynamical or semiclassical limit we investigated the fluctuations in the eigenvalue spectra and length spectra, which exhibit peaks at the lengths of the periodic orbits emerging in that limit. Since the eigenvalues of isospectral QBs coincide, also their spectral properties are identical. Furthermore, it could be shown that their length spectra are the same [46]. This implies that the properties—such as the degree of chaoticity—of their classical dynamics are identical. The spectral properties of generic quantum systems with fully chaotic classical counterparts are well described by those of random matrices [47] from the Gaussian orthogonal ensemble (GOE) when time-reversal symmetry is preserved, and from the Gaussian unitary ensemble (GUE) when it is violated [48–50], whereas those of quantum systems with an integrable classical counterpart behave like Poissonian random numbers [51]. It was shown in [45] that NBs which do not possess any geometric symmetries are not time-reversal invariant, implying that their spectral properties coincide with those of random matrices from the GUE if the NB has the shape of a billiard with chaotic classical dynamics. Polygonal QBs like the ones analyzed in the present article may exhibit Poissonian, GOE, or nonuniversal intermediate statistics. The latter case occurs, e.g., for pseudointegrable billiards [52] of which the boundary comprises corners with angles that are rational multiples of π , like in the examples shown in Fig. 1. It was shown that, despite the presence of diffractive orbits originating from these corners, the length spectra of isospectral QBs are identical. Accordingly, the question arose how strong the effect of the corners is on the spectral properties of the corresponding NBs, especially, whether not only their eigenvalues but also the fluctuations in their spectra and the length spectra are distinct.

Section II briefly reviews the transplantation method which is generally used to construct nonisometric pairs of isospectral QBs with Dirichlet, Neumann, or mixed boundary conditions. In Sec. III we outline why the transplantation method is not applicable for NBs and then illustrate nonisospectrality in Sec. IV for various shapes which are known to correspond to isospectral QBs. The results on the spectral properties and length spectra are presented in Sec. V. Our findings are summarized and discussed in Sec. VI.

II. CONSTRUCTION OF NONISOMETRIC ISOSPECTRAL PLANAR QBs WITH THE TRANSPLANTATION METHOD

We illustrate in Fig. 1 how the billiard shown in (b) is obtained from that depicted in (a) by applying the transplantation method which was used to construct all known nonisometric and isospectral planar billiards and introduced by Bérard [11]. These are composed of several identical base tiles which have three noncollinear straight-edge parts, which either form common edges of, respectively, two of the building blocks or part of the boundary of the billiard. In the examples shown in Fig. 1 the building block is an equilateral right-angle triangle. The eigenenergies and eigenfunctions of the corresponding QB with domain Ω are obtained by solving the free-space Schrödinger equation and imposing either Neumann (N) or

Dirichlet (D) boundary conditions or a mixture of them [5,6] on the wave functions along the boundary $\partial\Omega$,

$$\hat{H}_{QB}\psi(\mathbf{r}) = -\Delta_{x,y}\psi(\mathbf{r}) = k^2\psi(\mathbf{r}), \quad \mathbf{r} \in \Omega, \quad (1)$$

$$\psi(\mathbf{r} \in \partial\Omega) = 0 \quad (\text{D}), \quad (2)$$

$$\partial_n\psi(\mathbf{r} \in \partial\Omega) = 0 \quad (\text{N}),$$

with $k = \sqrt{\frac{2mE}{\hbar^2}}$ denoting the wave number associated with the eigenenergy E . We consider here for the illustration of the transplantation method the case of hard-wall boundaries, that is, Dirichlet boundary conditions. The essential idea of this method is to construct the eigenfunctions of a billiard from those of a nonisometric one with the same boundary conditions by translating and superimposing the wave function components denoted by $\psi_T(\mathbf{r})$ if $\mathbf{r} \in T$ with $T = A, B, \dots, G$, while ensuring that their superposition fulfills the Dirichlet condition along the boundary of the new domain and is continuous and has a continuous normal derivative at the common edges of the building blocks. For example, to construct the wave function component in building block a of the domain shown in Fig. 1(b) the three building blocks D, E, G (and their wave functions) of that shown in (a) were moved to domain a and arranged such that similar edges, that is, edges plotted as dashed, dotted, and solid lines, respectively, were on top of each other. For this the building block E needed to be flipped about its dotted edge. Accordingly, it is denoted by \bar{E} . This procedure corresponds to a unitary mirror reflection of a wave function about the associated edge so that the original and the new wave function are either symmetric or antisymmetric to each other with respect to the mirror axis. Furthermore, since the Schrödinger equation satisfied by the wave functions in each building block of the original billiard is linear, any linear combination of translations of these wave functions will be a solution of it with the same eigenvalue. Hence, in order to construct billiards which are nonisometric with respect to the original one, yet have identical eigenenergies, linear combinations of the wave function components inside the building blocks need to be found which vanish along the billiard boundary and are continuous and have a continuous normal derivative at the common edges of the building blocks. In Ref. [15] Chapman introduced a simple procedure which corresponds to realizing the transplantation method by using paper folding and stacking. For this several copies of the original billiard shape are folded along the edges of the building blocks in various ways, stacked on top of each other, and then the wave functions are superimposed [2] where a minus sign is assigned to wave function components in building blocks which had to be folded in order to adjust the wave functions to the new building block. The billiard shown in Fig. 1(b) is obtained with the paper-folding method by taking three copies of the domain (a) [2,15].

III. FAILURE OF THE TRANSPLANTATION METHOD FOR NBS

In the relativistic case, the massless spin-1/2 particle is confined to a bounded two-dimensional domain in the (x, y) plane by imposing boundary conditions on the two-

component spinor $\psi = \begin{pmatrix} \psi_1 \\ \psi_2 \end{pmatrix}$, where we chose those introduced in Ref. [45] for NBs. Defining the boundary $\mathbf{r}(s)$ of the NB in the complex plane by $z(s) = x(s) + iy(s)$ through the arc-length parameter $s \in [0, \mathcal{L}]$ with \mathcal{L} denoting the perimeter, confinement to the billiard domain is achieved with the boundary condition that there is no outward flux, yielding

$$\hat{\mathbf{n}} \cdot \mathbf{j}[\mathbf{r}(s)] = \hat{\mathbf{n}} \cdot [\psi^\dagger \nabla_p \hat{H}_{NB} \psi]|_{\partial\Omega} = 0. \quad (3)$$

Here, $\hat{\mathbf{n}}$ denotes the outward normal to the boundary and $\mathbf{j}(\mathbf{r}) = c(\text{Re}[\psi_1^*(\mathbf{r})\psi_2(\mathbf{r})], \text{Im}[\psi_1^*(\mathbf{r})\psi_2(\mathbf{r})])$ the expectation value of the current operator $\hat{\mathbf{j}} = \nabla_p \hat{H}_{NB}$ at \mathbf{r} . Accordingly, the Dirac equation of neutrino billiards is given in terms of the wave number k , $E = \hbar ck$, by

$$\begin{aligned} \hat{H}_{NB}\psi &= -i \begin{pmatrix} 0 & \frac{\partial}{\partial x} - i \frac{\partial}{\partial y} \\ \frac{\partial}{\partial x} + i \frac{\partial}{\partial y} & 0 \end{pmatrix} \psi \\ &= k\psi, \quad \mathbf{r} \in \Omega, \end{aligned} \quad (4)$$

$$\psi_2(s) = iB(s)e^{i\alpha(s)}\psi_1(s), \quad \mathbf{r} \in \partial\Omega, \quad (5)$$

where $\alpha(s)$ corresponds to the angle of $\hat{\mathbf{n}}(s)$ with respect to the x axis at $\mathbf{r}(s)$. We chose as in Ref. [45] for infinite-mass confinement $B(s) = 1$, which implies that the current flows for *all* eigenstates in the same rotational direction along the boundary. The boundary condition Eq. (5) links the wave function components $\psi_j(s)$, $j = 1, 2$ along the boundary.

The transplantation method uses the fact that a mirror symmetry of a QB implies that its wave functions are either symmetric or antisymmetric with respect to the associated symmetry axis, that is, fulfill there the Neumann, respectively, Dirichlet boundary condition. However, the Dirac Hamiltonian \hat{H}_{NB} is not invariant under mirror reflection operation, implying that the eigenfunctions of a NB generated by reflection of a building block at one of its straight line segments cannot be classified according to their symmetry properties with respect to the reflection axis. If the latter is chosen along the x or y axis the corresponding unitary reflection operators are $\hat{U}_x = \hat{\sigma}_x$ and $\hat{U}_y = i\hat{\sigma}_y$, respectively. Then the eigenfunctions of the transformed Hamilton operator

$$\hat{H}'_{NB} = \hat{U}^\dagger \hat{H}_{NB} \hat{U} \quad (6)$$

are obtained from those of \hat{H}_{NB} , denoted by $\psi = \begin{pmatrix} \psi_1 \\ \psi_2 \end{pmatrix}$, as [53]

$$\tilde{\psi}_x = \begin{pmatrix} \tilde{\psi}_{x,1} \\ \tilde{\psi}_{x,2} \end{pmatrix} = \begin{pmatrix} \psi_2 \\ \psi_1 \end{pmatrix}, \quad \tilde{\psi}_y = \begin{pmatrix} \tilde{\psi}_{y,1} \\ \tilde{\psi}_{y,2} \end{pmatrix} = \begin{pmatrix} -\psi_2 \\ \psi_1 \end{pmatrix}. \quad (7)$$

In the transformed coordinate system the normal vector becomes $e^{i\tilde{\alpha}} = e^{-i\alpha}$ for \hat{U}_x and $e^{i\tilde{\alpha}} = -e^{-i\alpha}$ for \hat{U}_y . Invariance with respect to these reflection operations, and thus any combination of them, holds if the transformed eigenfunction components of \hat{H}_{NB} also fulfill the boundary condition

$$\tilde{\psi}_2(\phi) = i e^{i\tilde{\alpha}(\phi)} \tilde{\psi}_1(\phi), \quad (8)$$

which obviously is not the case. This implies that a wave function obtained by reflections of those in the building blocks won't be an eigenfunction of \hat{H}_{NB} , which is crucial for the construction of nonisometric isospectral billiard pairs with the transplantation method.

Note that $\hat{H}_{NB}(-x, y) = \hat{H}_{NB}^*(x, y)$ and $\hat{H}_{NB}(x, -y) = \hat{\sigma}_z \hat{H}_{NB}^*(x, y) \hat{\sigma}_z$, with the star denoting complex conjugation, that is, the effect of the unitary reflection operations \hat{U}_x or \hat{U}_y is equivalent to that of a generalized antiunitary operator of the form $\hat{T} = \hat{U} \hat{K}$ with \hat{U} and \hat{K} denoting a unitary operator and complex conjugation, respectively. Thus some of the reflected wave functions will have the properties $[\psi_1(-x, y), \psi_2(-x, y)] = \pm[\psi_1^*(x, y), \psi_2^*(x, y)]$ and $[\psi_1(x, -y), \psi_2(x, -y)] = \pm[\psi_1^*(x, y), -\psi_2^*(x, y)]$, respectively, i.e., will correspond up to a possible sign to the complex conjugates of the original wave functions, which comply with the boundary condition Eq. (5). However, since the operator \hat{T} is not unitary this is not necessarily the case. Nevertheless, as can be seen from these relations, even in these cases the real and imaginary parts of the wave function components ψ_1 and ψ_2 transform differently under reflection as dictated by the boundary condition Eq. (5).

Furthermore, the Dirac Hamiltonian \hat{H}_{NB} of a NB with two perpendicular symmetry axes is invariant under rotations by π . Accordingly, the components ψ_1 and ψ_2 , resulting from two consecutive reflections of those in the interior of, e.g., the building block of domains 1 and 2 in Fig. 1 at the two perpendicular straight-line edges, and the original components would be symmetric and antisymmetric to each other, respectively, or vice versa with respect to a rotation by π at the common corner. However, generally, a procedure consisting only of such rotations is not sufficient to realize pairs of nonisometric isospectral billiards.

Failure of the transplantation method may be attributed to the additional spin degree of freedom which is not appropriately accounted for and to the chirality property which leads to the discrepancies under the reflection operation. Indeed, the direction of the flow at the boundary is fixed for all eigenstates of a NB by the choice of $B(s)$ in Eq. (5) and reversed when applying a reflection operation which would correspond to a change of sign of $B(s)$. Consequently, the construction of wave functions which fulfill the boundary conditions, that is, exhibit unidirectionality of the flow along the boundary, and are continuous and have continuous normal derivatives along the common edges of the building blocks is not possible through purely geometric operations. In the following section we report on the numerical analysis of two pairs of NBs with the shapes of isospectral QBs.

IV. NUMERICAL EVIDENCE OF NONISOSPECTRALITY FOR NBS WITH THE SHAPES OF ISOSPECTRAL QBS

We used the boundary integral method for the computation of the eigenstates of the NBs since, in contrast to other numerical methods, it incorporates the boundary conditions and reduces the two-dimensional eigenvalue problem to an integral equation along the boundary. Yet, it is known that due to the presence of inner corners in polygonal QBs like the ones shown in Fig. 1, it is an intriguing task to obtain the eigenvalues with high precision. Accordingly, for comparison of numerical results and the test of accuracy we also used this method for the determination of the eigenstates of the corresponding QBs. In order to overcome the problems associated with corners present when using the boundary integral

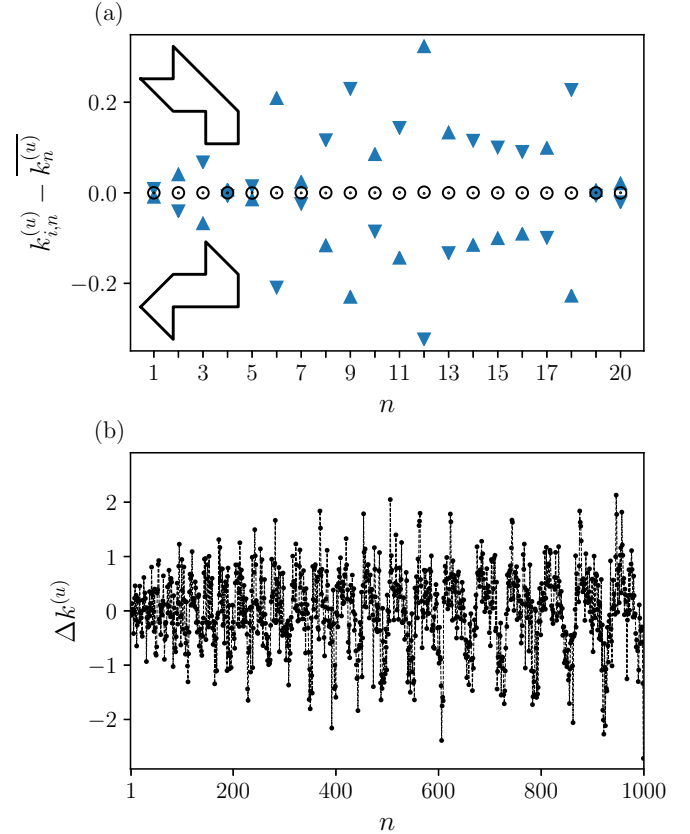


FIG. 2. (a) First 20 unfolded eigenvalues $k_{i,n}$, $i = 1, 2$ of domains 1 and 2 depicted in Fig. 1 for the QBs (dots and circles for domains 1 and 2, respectively) and the NBs (triangles down and up for domains 1 and 2, respectively) for $b = 80$. Here, the average value $\bar{k}_n = (k_{1,n} + k_{2,n})/2$ was subtracted from the associated eigenvalues. (b) The difference $\Delta k^{(u)} = (k_{1,n}^{(u)} - k_{2,n}^{(u)})$ versus n of the first 1000 unfolded eigenvalues of the NBs with the shapes shown in Fig. 1. The number of quadrature points equaled $b = 80$.

method we applied a regularization procedure [20,54]. For the interested reader it is reviewed in Appendix A. For the computation of the eigenstates of the corresponding NBs we employed the expanded boundary integral method [53]. Information on the case of NBs with corners and on the extension of the regularization procedure for QBs to NBs is provided in Appendix B.

We computed the first 1000 eigenvalues of QBs and NBs with the shapes of domains 1 and 2 in Fig. 1 solving Eqs. (A6) and (B6), where we chose the same number N of Gauss-Legendre quadrature points for both cases. The former are known to be isospectral. Accordingly, we used the differences of the eigenvalues of the two QBs as an additional measure for the numerical accuracy for both cases and also in order to decide whether those between close-lying eigenvalues of the two NBs are due to numerical inaccuracy or indicate nonisospectrality. In panel (a) of Fig. 2 the first 20 eigenvalues of the two QBs and NBs are plotted. Here, we subtracted from the eigenvalues $k_{i,n}^{(u)}$, $i = 1, 2$ corresponding to domains 1 and 2, respectively, their average $\bar{k}_n = (k_{1,n}^{(u)} + k_{2,n}^{(u)})/2$. While the shifted eigenvalues of the QBs marked by dots and circles, respectively, all are close to zero, those of the NBs

TABLE I. Comparison of the first 20 eigenwave numbers obtained for the two shapes shown in Fig. 1 for the nonrelativistic and the relativistic cases, respectively.

No.	QB			NB		
	Domain 1	Domain 2	Δ	Domain 1	Domain 2	Δ
1	3.18706	3.18682	-0.00025	1.75309	1.73430	-0.01879
2	3.82432	3.82448	0.00016	2.28064	2.34326	0.06262
3	4.55001	4.54986	-0.00015	3.11267	3.03381	-0.07885
4	5.11373	5.11371	-0.00002	3.65205	3.65844	0.00639
5	5.38449	5.38448	-0.00001	4.09310	4.07982	-0.01328
6	6.06938	6.06938	-0.00000	4.60576	4.76562	0.15986
7	6.51062	6.51061	-0.00001	4.98236	4.99969	0.01732
8	6.79453	6.79451	-0.00002	5.24984	5.16930	-0.08054
9	7.02485	7.02485	0.00000	5.59598	5.44636	-0.14962
10	7.22599	7.22597	-0.00003	5.85172	5.90382	0.05210
11	7.56674	7.56673	-0.00001	6.17963	6.09573	-0.08390
12	7.96777	7.96772	-0.00005	6.43579	6.61390	0.17811
13	8.23207	8.23207	-0.00000	6.65991	6.73070	0.07080
14	8.40600	8.40600	-0.00000	7.02229	6.96273	-0.05956
15	8.71348	8.71340	-0.00008	7.27651	7.22720	-0.04931
16	9.13948	9.13947	-0.00000	7.67091	7.62805	-0.04286
17	9.21914	9.21908	-0.00006	7.79204	7.83741	0.04537
18	9.43037	9.43035	-0.00002	8.10593	8.00462	-0.10131
19	9.73885	9.73885	-0.00000	8.21310	8.21551	0.00241
20	9.89530	9.89530	-0.00000	8.30338	8.31231	0.00893

corresponding to triangles up and down, respectively, clearly deviate from each other except for a few cases like for $n = 4$ and $n = 19$. The obtained eigenwave numbers of the four billiards are listed in Table I. The distances between the eigenvalues of the QBs are all less than 0.0001 for $n > 3$, whereas in the NBs they are typically larger than 0.01. The reason for these deviations from zero cannot be attributed to the numerical inaccuracy of the eigenvalues; see Fig. 17. In Fig. 2(b) we show the differences of corresponding unfolded eigenvalues of domains 1 and 2. The distances are considerably larger than their numerical inaccuracy and typically of the order of $\simeq 0.3$ mean spacings. Thus we may conclude that, in contrast to the QBs, the NBs with the shapes of domains 1 and 2 of Fig. 1 are not isospectral.

To corroborate these findings, we furthermore analyzed the eigenvalue spectra of NBs with the shapes of warped propellers [16] depicted in the insets of Fig. 3(a). The corresponding QBs were shown to be isospectral and, indeed, the unfolded eigenvalues $k_{i,n}^{(u)}$ shown as dots and circles, respectively, coincide within the numerical error. In contrast, for the NBs the distance between corresponding eigenvalues $k_{1,n}^{(u)}$ and $k_{2,n}^{(u)}$ plotted as triangles up and down, respectively, is typically considerably larger than 0.05 on the scale of the mean spacing, as also demonstrated in Fig. 3(b) for the first 1000 unfolded eigenvalues, and thus may not be attributed to the numerical inaccuracy which is similar to that for the domains shown in Fig. 1 (see Fig. 17). Accordingly, NBs with the shapes of these warped propellers are also not isospectral, even though Dirichlet isospectrality has been proven based on the transplantation method for the corresponding QBs [16].

In order to gain further insight into the differences between isospectral QBs and NBs of corresponding shapes, we

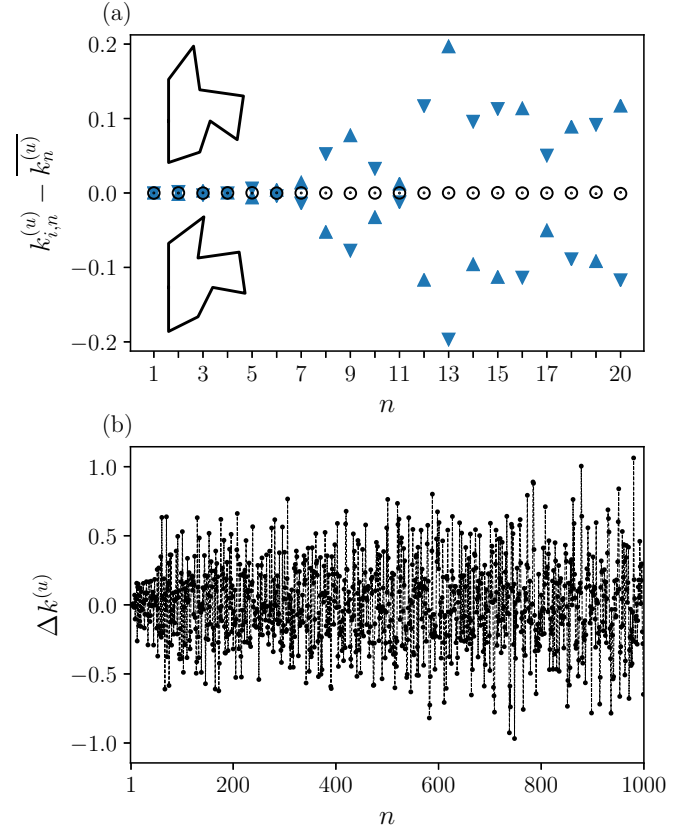


FIG. 3. Same as in Fig. 2 for the pair of billiards shown in the insets in panel (a). Their isospectrality was demonstrated for the nonrelativistic case in [16].

furthermore computed wave functions. A few examples for the domains shown in Fig. 1 are plotted in Fig. 4. The top row presents the intensity distributions $|\psi_n(\mathbf{r})|^2$ for the states $n = 1, 9, 19$ of the QBs and the middle row the corresponding ones, $|\psi_n(\mathbf{r})|^2 = |\psi_{1,n}(\mathbf{r})|^2 + |\psi_{2,n}(\mathbf{r})|^2$ of the spinor wave functions $\psi(\mathbf{r}) = \begin{pmatrix} \psi_1(\mathbf{r}) \\ \psi_2(\mathbf{r}) \end{pmatrix}$ of the NBs. While the intensity distributions of the QBs exhibit clear nodal-domain patterns, this is not the case for the NBs, the reason being that the wave functions are real in the former case, whereas the spinor components $\psi_j(\mathbf{r})$, $j = 1, 2$ of $\psi(\mathbf{r})$ are complex [55,56]. Consequently, their absolute values at most possess nodal points, as illustrated for the 19th eigenstate in Fig. 5. Indeed, the real and imaginary parts of the two wave function components, which are depicted in the first and second row, obey along the boundary different boundary conditions, as can be checked by separating that for the wave function given in Eq. (5) accordingly. Furthermore, they exhibit nodal lines which are at distinct locations. This is demonstrated in Appendix C. Consequently, $|\psi_j(\mathbf{r})|$, $j = 1, 2$ only vanishes at crossings of the nodal lines of its real and imaginary parts, as illustrated in the third row of Fig. 5. Note that, for this example, the imaginary part of $\psi_1(\mathbf{r})$ is small compared to the real part, so that the structure of $|\psi_1(\mathbf{r})|$ is similar to that of the latter. The fourth row shows the phases of $\psi_j(\mathbf{r}) = |\psi_j(\mathbf{r})|e^{i\arg(\psi_j)}$, $j = 1, 2$. The nodal points, where $\arg(\psi_j)$ experiences a jump from $0 \rightarrow \pm\pi$ along the nodal lines of the imaginary part of $\psi_j(\mathbf{r})$

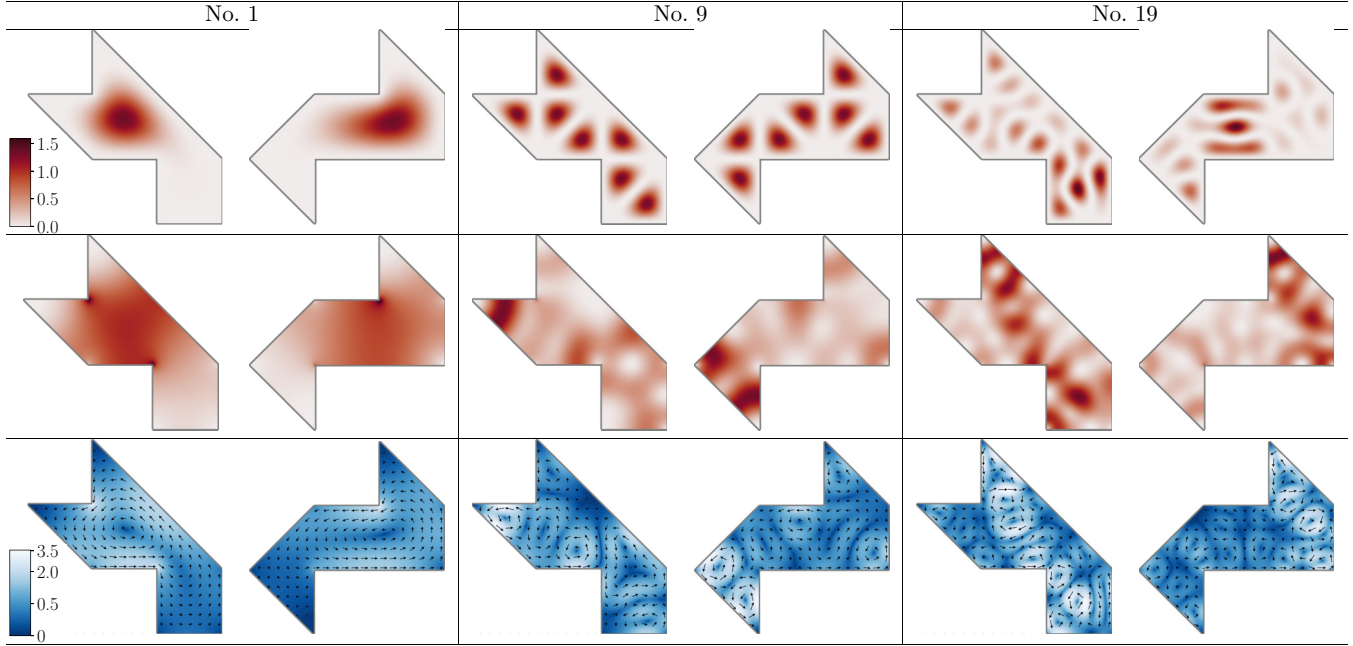


FIG. 4. First row: density plots of $|\psi|^2$ for the first, ninth, and 19th pairs of eigenstates of the nonrelativistic isospectral QBs with the shapes of domains 1 and 2 in Fig. 1. The wave functions exhibit clearly visible nodal-domain patterns. Second row: density plots of $|\psi|^2 = |\psi_1|^2 + |\psi_2|^2$ of the spinor wave functions of the corresponding NBs for the first, ninth, and 19th eigenstate. Third row: the associated local currents $|\mathbf{j}|$. They also show clear nodal-domain patterns which are absent in the density plots of $|\psi|^2$.

and from $-\pi/2$ to $\pi/2$ along those of the real part, are clearly visible.

In a NB boundary conditions are not imposed on the wave functions, but on the normal component of the current. Therefore, one should also consider the current structure inside the billiard. The modulus square of the current, $|\mathbf{j}(\mathbf{r})|^2$, associated with the states $n = 1, 9, 19$ of the NBs with shapes shown in Fig. 1 is shown in the bottom row of Fig. 4. In contrast to the intensity distribution of the wave function it exhibits a clear structure which is formed by the vortices of the flow and is similar to that exhibited by the wave functions of the corresponding QB. Yet, as will be outlined in more detail in Sec. V, we were not able to identify eigenstates of the NB possessing a vanishing normal flow along the edges of all building blocks, which would be the analog of the trivial wave functions of the corresponding QBs mentioned at the beginning of Sec. II, one example being wave function no. 9 in Fig. 4, which corresponds to a combination of the lowest eigenstates of the individual triangular building blocks.

As visible in Fig. 4, the wave functions associated with the first eigenstate of the NBs have a strong support at the diffracting corners for the first eigenstate. The associated boundary wave function shown in Fig. 16 exhibits sharp peaks at the diffractive corners, which might induce a large numerical error in the determination of the corresponding eigenvalue when using Eq. (B4). However, as outlined in detail in Appendix B, the impact of these discontinuities on the numerical accuracy in the determination of the eigenstates is smaller for NBs than it is for QBs. This corroborates our assumption that the observed nonisospectrality may not be attributed to numerical inaccuracies.

V. FLUCTUATION PROPERTIES IN THE EIGENVALUE SPECTRA OF THE NBS

We also investigated the spectral properties and the length spectra of the pairs of NBs and compared them with those of the corresponding QBs. In the latter case the spectral properties evidently coincide for each pair. Accordingly, a central question was whether not only the eigenvalues but also the fluctuations in the eigenvalue spectra are different in the relativistic case.

As mentioned in the Introduction, the spectral properties of QBs with shapes of domains 1 and 2 in Fig. 1 are nonuniversal. They had been studied in [57]. After removal of all trivial wave functions, which constituted about 13% of the 598 eigenvalues, the authors found good agreement with GOE statistics. This implies that the eigenvalue spectra are composed of regular eigenstates corresponding to the trivial wave functions and chaotic ones of which the wave functions are spread over the whole billiard area. The fact that the eigenvalues corresponding to the trivial wave functions can be simply taken out of the spectra to achieve good agreement with GOE implies that they are only weakly correlated with the nontrivial ones. Accordingly, a random matrix ensemble composed of eigenvalues from the GOE and Poissonian random numbers describes the spectral properties of the spectrum comprising all 598 eigenvalues [58–60] well.

We investigated the fluctuation properties in the eigenvalue spectra of NBs with these shapes and also of the pair of isospectral propellor billiards shown in the insets of Fig. 3(a). We analyzed short-range correlations in terms of the nearest-neighbor spacing distribution $P(s)$ and the cumulative nearest-neighbor distribution $I(s)$, and long-range correlations in

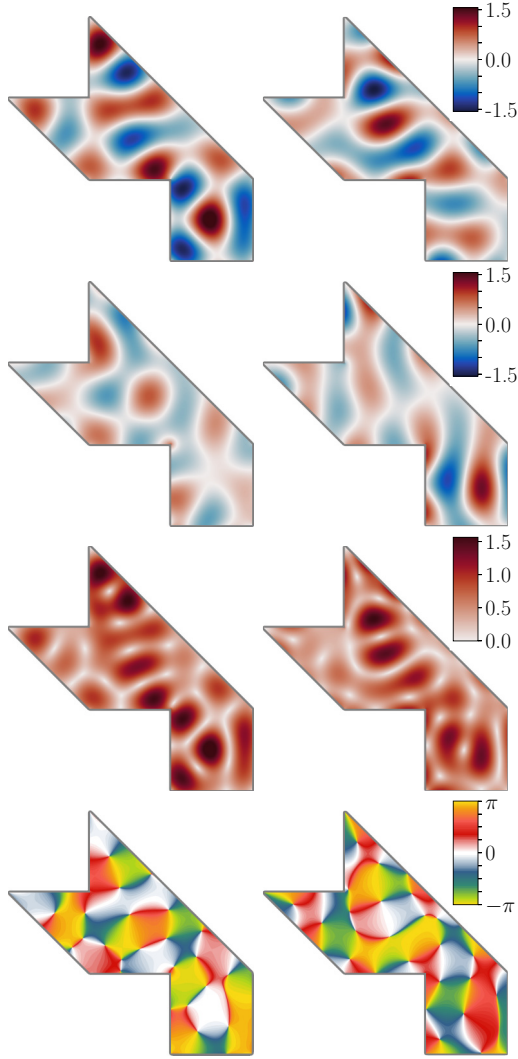


FIG. 5. Wave function components corresponding to the 19th eigenstate of the NBs with the shape of domain 1 in Fig. 1. From up to down are shown the real part, the imaginary part, and modulus and phase of $\psi_j = |\psi_j|e^{i\arg(\psi_j)}$, respectively. The left column shows the first component ($j = 1$) and the right one the second one ($j = 2$).

terms of the number variance $\Sigma^2(L)$ and the spectral rigidity $\Delta_3(L)$ [47] of the unfolded eigenvalues. Figure 6 shows the fluctuating part of the integrated spectral density, $N^{\text{fluc}}(k_n) = N(k_n) - N^{\text{Weyl}}(k_n)$ and Fig. 7 exhibits the results for the NBs with the shapes of domains 1 and 2 in Fig. 1. The curves for domain 1 (red full lines and triangles up) and domain 2 (green dashed line and triangles down) differ slightly but deviations are clearly visible. For the short-range correlations the spectral properties are close to the corresponding GUE curves, whereas notable deviations from GUE statistics are visible for the long-range correlations. To identify the origin of this behavior, we computed the associated wave functions and currents and found several which are strongly localized along classical periodic orbits that bounce back and forth between opposite sides as in the first example in Fig. 8 or between three or four sides as in the other three examples, that is, they exhibit the same feature as the bouncing-ball orbits in the stadium billiard [61] and thus might be responsible for

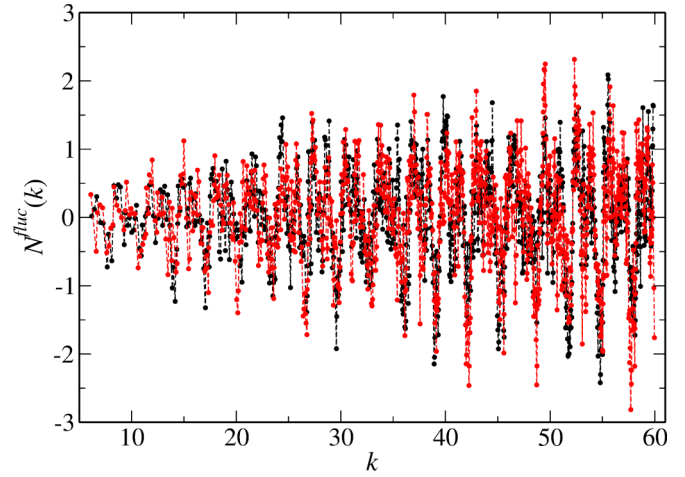


FIG. 6. Fluctuating part of the integrated spectral density of domains 1 (black) and 2 (red) shown in Fig. 1.

the deviations of the spectral properties from GUE behavior observed in Fig. 7. Their presence is reflected by the slow oscillations visible in Figs. 2 and 6 and their effect on the spectral statistics is similar to that of the trivial eigenstates in the corresponding QBs.

To verify whether the deviations of the long-range correlations in Fig. 7 from GUE behavior are due to these bouncing-ball orbit type states, we accordingly compared

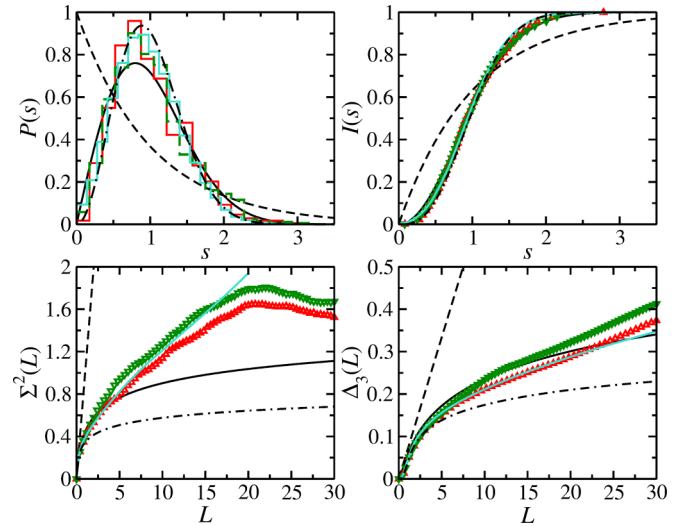


FIG. 7. Spectral properties of the NBs with the shapes of domains 1 and 2 shown in Fig. 1 (red [solid line histogram and triangles up] and green [dashed line histogram and triangles down], respectively). Shown are the nearest-neighbor spacing distribution $P(s)$, the integrated nearest-neighbor spacing distribution $I(s)$, the number variance $\Sigma^2(L)$, and the spectral rigidity $\Delta_3(L)$. The dashed lines, full lines, and dash-dotted lines show the corresponding curves for Poisson, GOE, and GUE statistics, respectively. The curves agree well with the turquoise ones which were obtained from level sequences composed of eigenvalues of random matrices from the GUE and a 6% admixture of Poissonian random numbers (see main text).

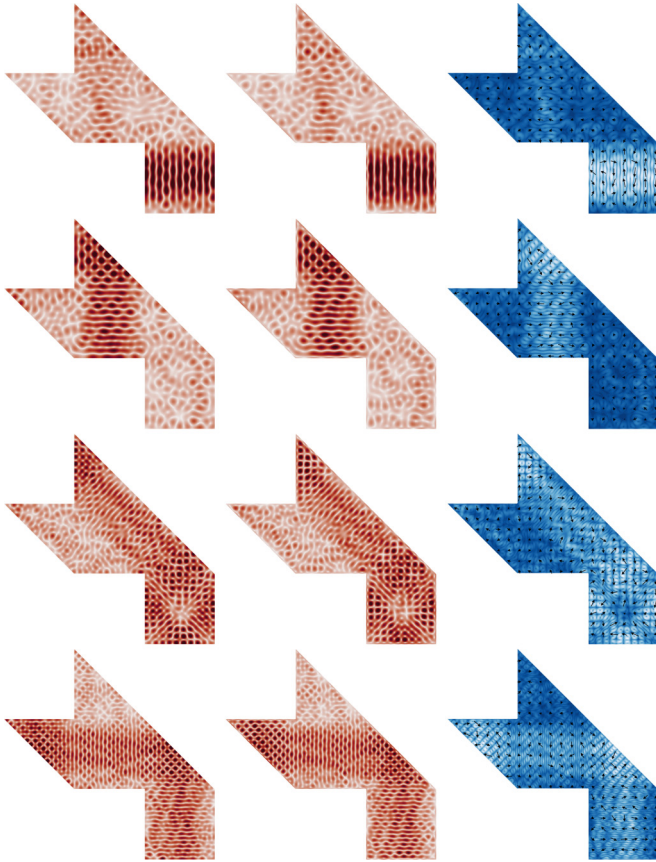


FIG. 8. $|\langle\psi_{1,n}\rangle|$ (first column), $|\langle\psi_{2,n}\rangle|$ (second column), and current (third column) for the eigenstates $n = 305, 335, 573, 808$ from up to down of the NB with the shape of domain 1 in Fig. 1. For this shape and also domain 2 we found many wave functions which are uniformly distributed over the whole billiard area, but also some which are localized on bouncing-ball orbits as illustrated in this figure.

their spectral properties to those of eigenvalue sequences generated from random matrices from the GUE and Poissonian random numbers and indeed found good agreement with the curves corresponding to domain 1 for the case where the latter constituted 6% of the spectrum, and for a slightly higher percentage for domain 2. This result corroborates our assumption that the bouncing-ball orbit type eigenstates are weakly coupled with the remaining ones which behave like those of quantum systems with classically chaotic dynamics and violated time-reversal invariance.

We also analyzed the spectral properties of the propellor-shaped NBs. The results are shown in Fig. 9. Again, the curves for the two NBs differ; however, the deviations are smaller than in Fig. 7. In this case, we found good agreement with GUE statistics. Indeed, for this case the fluctuating part of the integrated spectral density shown in Fig. 10 doesn't exhibit slow oscillations and we found only very few wave functions which are localized along bouncing-ball-like orbits.

It was demonstrated [46] that trajectories in billiard (a) in Fig. 1 which hit the diffractive corners do not have a counterpart in billiard (b). Still, as expected for isospectral QBs, the length spectra—that is, the modulus of the Fourier transform

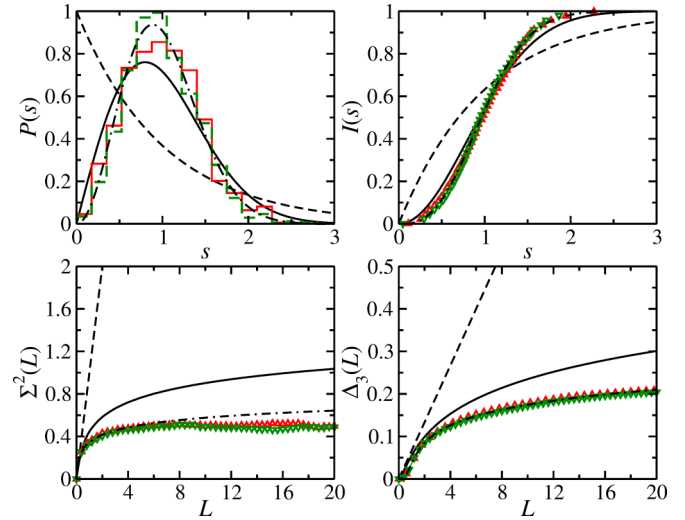


FIG. 9. Same as Fig. 7 for the NBs with the shapes shown in the insets of panel (a) of Fig. 3.

of the fluctuating part of the spectral density, which exhibits peaks at the lengths of classical periodic orbits—coincide. This property is referred to as “isolength spectrality” and implies that there is a correspondence between the diffractive trajectories of the two billiards. It was identified and shown to be a consequence of the transplantation property used to construct all known planar isospectral billiards in Ref. [46]. Thus such diffractive trajectories do not destroy isospectrality and isolength spectrality. In Figs. 11(a) and 11(b) we compare the length spectra for the NBs with the shapes of domains 1 and 2 in Fig. 1 and of the domains depicted in the insets of Fig. 3(a), respectively. They clearly confirm that NBs besides being nonisospectral do not possess isolength spectrality. In both cases, the pairs of NBs exhibit essentially peaks at the same positions, that is, periodic orbits of the same length, yet the amplitudes and, accordingly, the weights of their contributions in the ray-dynamical limit deviate considerably.

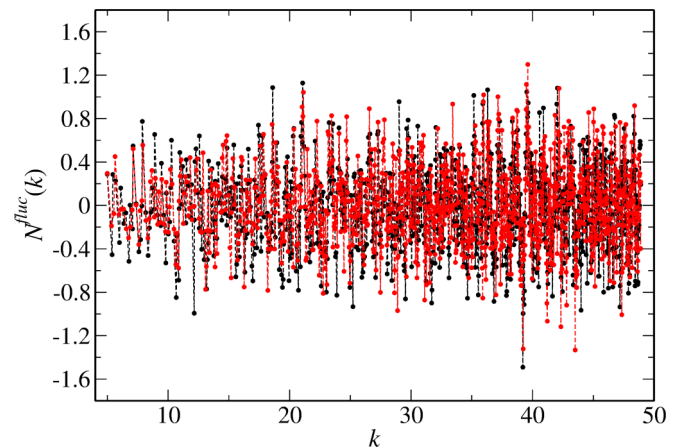


FIG. 10. Fluctuating part of the integrated spectral density of the NBs shown in the upper (black) and lower (red) insets of panel (a) of Fig. 3.

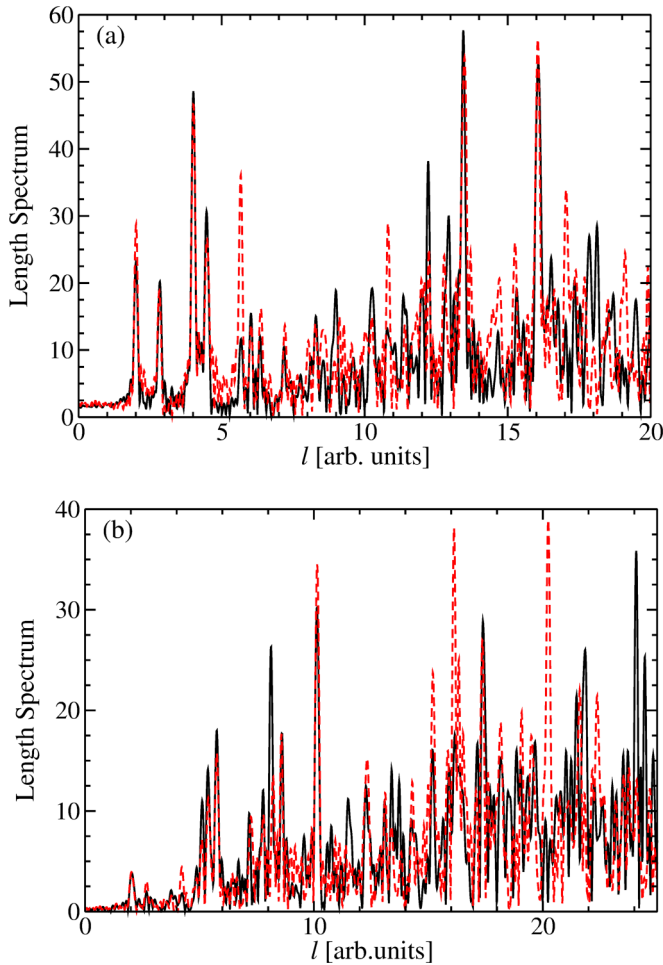


FIG. 11. Length spectra for the NBs with the shapes of domains 1 and 2 shown in Fig. 1(a) (black solid line and red dashed line, respectively) and in the insets of Fig. 3(a) (black solid line and red dashed line, respectively). They only agree, e.g., at peaks corresponding to bouncing ball orbits. Thus the eigenvalue spectra are neither isospectral nor isolength spectral.

VI. CONCLUSION

We have revisited Kac's famous question for massless spin-1/2 particles confined to a planar domain. To be more explicit, we investigated the properties of the eigenvalues and eigenfunctions of nonisometric pairs of NBs which are known to be Dirichlet and Neumann isospectral in the corresponding nonrelativistic QBs and illustrate in detail that isospectrality and also isolength spectrality are no longer present in the relativistic case. For this, we performed numerical high-precision calculations using the expanded boundary integral method [53]. The quantization of billiards with the shapes of the domains shown in Figs. 1 and 3 is a challenging task, so that the achievement of the high accuracy exhibited, e.g., in Fig. 17 is not self-evident and corroborates the efficiency of that method. Isospectral pairs of QBs are constructed on the basis of the transplantation method. The origin of the failure of isospectrality in the corresponding NBs is due to that of this method, since it does not take into account the additional spin degree of freedom and the chirality property [45] for

NBs. Actually, as outlined in Sec. III, the Dirac Hamiltonian with the boundary condition Eq. (5) for NBs is not invariant under mirror reflection. Thus the reflection operations applied in the transplantation method to the wave functions in the building blocks do not generate wave functions with the same eigenvalue except if two consecutive reflections are performed with respect to two perpendicular axes, which is crucial for the construction of nonisometric isospectral pairs of billiards.

The spectral properties of the pair of isospectral QBs shown in Fig. 1 were demonstrated to be well described by a random-matrix ensemble consisting of an admixture of eigenvalues of matrices from the GOE and of Poissonian random numbers accounting for chaotic eigenstates and the trivial ones, respectively. We found a similar behavior for the eigenvalues of the corresponding NBs, except that the spectral properties of the chaotic part of the eigenvalue spectrum coincides with those of matrices from the GUE and that the trivial eigenstates correspond to bouncing-ball modes. However, the spectral properties and also the amplitudes in the length spectra differ; that is, the pairs of NBs correspond to distinct relativistic quantum systems with differing ray-dynamical limits.

As mentioned in the Introduction, the field of relativistic quantum chaos arose with the fabrication of two-dimensional graphene sheets which exhibit relativistic phenomena in the vicinity of the touch points of the conduction and valence band [40,41], which are generally referred to as Dirac points. These features are attributed to the honeycomb lattice structure which is composed of two interpenetrating triangular lattices. At the touch points the electronic excitations are governed by a four-dimensional Dirac equation, comprising the Dirac operators for massless Dirac fermions associated with the two independent triangular lattices. On the grounds of Ref. [45], the spectral properties of chaotic graphene billiards (GBs) were expected to follow GUE statistics. Numerical and experimental studies, however, revealed that they coincide with those of time-reversal invariant chaotic systems, as is the case for nonrelativistic Schrödinger billiards [29,30,32–35,38]. These discrepancies result from the intervalley scattering at the boundary of GBs [30], which induces a mixing and thus a coupling of the two independent Dirac equations.

We investigated the spectral properties of a pair of GBs with the shapes considered in the article in the regions of the band edges and the Dirac point, respectively, and found that (i) like the corresponding NBs, they are not isospectral, and (ii) their spectral properties coincide with those of matrices from a random-matrix ensemble consisting of an admixture of eigenvalues of matrices from the GOE and of Poissonian random numbers, respectively. Here, the ratio of the lengths of both spectra is similar to that found for the NBs. The result (i) is at a first glance in contradiction to the general supposition that, in the vicinity of the band edges, in good approximation, the eigenvalues and wave functions of GBs are directly related to those of the corresponding QBs [37,38,62]. While the wave functions of the pair of GBs associated with the lowest eigenstates are similar to those of the corresponding QBs, their eigenvalues do not coincide. Yet, this approximation is expected to become inapplicable when the deviations between the shape of a QB and the honeycomb lattice, i.e., GB, fitted into it become resolvable by the waves excited inside the

billiard. The two GBs with the shapes of the isospectral QBs considered in the present article, constructed by cutting out the shapes from a honeycomb lattice, always have distinct structures at the edges and thus differing boundary conditions. According to our numerical results these differences induce nonisospectrality starting from the bottom of the eigenvalue spectrum.

In the present article we consider NBs guided by the Dirac Hamiltonian for massless spin-1/2 particles with the boundary condition Eq. (5). However, the particles may also be confined to a planar domain by imposing different boundary conditions [63], which may have different chirality properties so that naturally the question arises of whether isospectrality may be encountered in such relativistic billiards. We came in Sec. III to the conclusion that the answer is no for relativistic billiards with the shapes of isospectral QBs, since the transplation method does not account for chirality and the additional spin degree of freedom.

ACKNOWLEDGMENTS

This work was supported by NNSF of China under Grants No. 11775100, No. 11775101, No. 11422541, and No. 11961131009. The work at Arizona State University is supported by the Vannevar Bush Faculty Fellowship program sponsored by the Basic Research Office of the Assistant Secretary of Defense for Research and Engineering and funded by the Office of Naval Research through Grant No. N00014-16-1-2828.

APPENDIX A: COMPUTATION OF THE EIGENSTATES OF QBs

While the isospectrality of a billiard composed of several copies of a building block and another one, constructed from it by applying the transplation method, can be proven mathematically, finding the eigenvalues and eigenfunctions is a challenging task. The only exceptions are trivial eigenstates of which the eigenfunctions fulfill the same boundary condition along the edges of *all* building blocks, that is, e.g., exhibit nodal lines there for the case of Dirichlet boundary conditions. For the determination of the other eigenstates a numerical procedure is needed which can cope with the unavoidable inner corners created when gluing together the building blocks. The basic idea of the method of particular solutions [2,64] is to use as an ansatz for the eigenfunctions an expansion around a diffracting corner with angle θ in terms of the solutions of the Schrödinger equation in polar coordinates, i.e., a sum of the form

$$\psi(r, \varphi) = \sum_l a_l J_{\frac{\pi l}{\theta}}(kr) \sin\left(\frac{\pi l}{\theta} \varphi\right), \quad (\text{A1})$$

which vanishes at the two edges connected to the corner [65]. However, this method fails if the billiard comprises more than one diffracting corner, yet was improved considerably in Ref. [66]. In Ref. [57] the mode matching method was applied to the two squares and three triangles forming the shapes shown in Fig. 1. A superposition of the known solutions in the five subdomains was used as ansatz and the associated amplitudes were determined by requiring that solutions of

the Dirichlet problem and their normal derivatives should be continuous at the boundaries separating the subdomains. This method, however, relies on the existence of analytic solutions of the Schrödinger equation inside the subdomains with Dirichlet and Neumann boundary conditions along their edges. In other numerical calculations the billiards were decomposed into subdomains with each one containing no more than one diffracting corner [67] and using as ansatz for the wave functions in these subdomains expansions in terms of Bessel functions as in Eq. (A1). Furthermore, to determine the superposition of the wave functions best approximating the eigenfunctions of the billiards an algorithm proposed in [68] was applied which avoids the singularities occurring when using the mode-matching method.

A standard method to compute the eigenvalues and eigenfunctions of a QB, of which the boundary $\mathbf{r}(s)$ is defined by an arc-length parameter s and is composed of a finite number of C^2 arcs $\Gamma_1, \Gamma_2, \dots, \Gamma_m$ bordered by m corners at $\mathbf{r}(s_i) = \mathbf{c}_i$, $i = 1, \dots, m$ with inner angles θ_i and of which the eigenfunctions satisfy Dirichlet boundary conditions, is to solve a boundary integral equation deduced from Green's theorem [54,69,70],

$$\frac{ik}{2} \oint_{\partial\Omega} ds Q(s', s; k) u(s) = \chi u(s'), \quad (\text{A2})$$

with

$$\chi = \begin{cases} 1, & \mathbf{r}(s') \in \partial\Omega \setminus \{\mathbf{c}_1, \mathbf{c}_2, \dots, \mathbf{c}_m\}, \\ \frac{\theta_i}{\pi}, & \mathbf{r}(s') = \mathbf{c}_1, \mathbf{c}_2, \dots, \mathbf{c}_m, \end{cases} \quad (\text{A3})$$

and $u(s) = \hat{\mathbf{n}}(s) \cdot \vec{\nabla} \psi[\mathbf{r}(s)]$ denoting the outward normal derivative of the wave function $\psi[\mathbf{r}(s)]$ and

$$Q(s', s; k) = -\hat{\mathbf{n}}(s') \cdot \frac{\mathbf{r}(s') - \mathbf{r}(s)}{\rho(s', s)} H_1^{(1)}(k\rho(s', s)), \quad (\text{A4})$$

where $H_1^{(1)}(k\rho(s, s'))$ is the order-one Hankel function of the first kind and $\rho(s', s) = |\mathbf{r}(s') - \mathbf{r}(s)|$. Note that for QBs the integrand of the boundary integral equation for the eigenstates has singularities so that, instead of analyzing the associated single layer equation, the double layer equation (A2) for the normal derivative of the wave function along the boundary is solved. It can be reduced to a matrix equation by discretizing the boundary parameter s with appropriate quadrature points $\{s_1, s_2, \dots, s_N\}$ and weights $\{w_1, w_2, \dots, w_N\}$, yielding

$$u(s_i) = \frac{ik}{2} \sum_{j=1}^N Q^{(N)}(s_i, s_j; k) w_j u(s_j). \quad (\text{A5})$$

This set of equations has a nontrivial solution if and only if

$$\det[\mathcal{A}^{(N)}(k)] = 0, \quad \mathcal{A}_{ij}^{(N)}(k) = \delta_{ij} - Q^{(N)}(s_i, s_j; k) w_j, \quad (\text{A6})$$

with δ_{ij} denoting the Kronecker δ . We chose the Gauss-Legendre quadrature, which is known to provide for a given N a more accurate approximation of line integrals than, e.g., an equidistant partition. The solutions are at discrete values $k = k_n$, $n = 1, 2, \dots$, and $k_1 \leq k_2 \leq k_3 \dots$. These are expected to approach the eigenvalues of the original Dirichlet problem with increasing discretization size N . An estimate of the required number of quadrature points N is given by

the number of k -dependent de Broglie wavelengths $\lambda_k = \frac{2\pi}{k}$ fitting into the perimeter \mathcal{L} , \mathcal{L}/λ_k . A measure for the accuracy of this procedure can be obtained either from the deviation of $|\det[\mathcal{A}^{(N)}(k_n)]|$ or of the original boundary integral equation for the wave functions, from which Eq. (A2) was deduced, $\oint_{\partial\Omega} ds u(s) G[\mathbf{r}(s'), \mathbf{r}(s); k_n] = 0$, from zero, with $G(\mathbf{r}', \mathbf{r}; k)$ denoting the free-space Green function. It, indeed, can be shown that, if the domain is piecewise smooth with no corners, $\det[\mathcal{A}^{(N)}(k)]$ converges for $N \rightarrow \infty$ and its zeros coincide with the sought-after eigenvalues. Only under these conditions the integral kernel $Q(s', s; k)$ is continuous so that Fredholm's theory applies, which guarantees this convergence. The reason is that the singularity of $H_1^{(1)}(k\rho(s, s'))$ approached for $s' \rightarrow s$,

$$H_1^{(1)}(k\rho(s', s)) \rightarrow -\frac{2i}{\pi k\rho(s', s)} + i\frac{k\rho(s', s)}{\pi} \ln\left[\frac{k\rho(s', s)}{2}\right] + O[k\rho(s', s)], \quad (\text{A7})$$

is compensated by the prefactor

$$\hat{\mathbf{n}}(s') \cdot \frac{\mathbf{r}(s') - \mathbf{r}(s)}{\rho(s', s)} \rightarrow \frac{1}{2}\kappa(s')\rho(s', s) + O[\rho(s', s)^2]. \quad (\text{A8})$$

Here, $\kappa(s)$ denotes the curvature of the boundary at s . However, the $1/\rho$ singularity of $H_1(k\rho)$ is not canceled when $\mathbf{r}(s)$ and $\mathbf{r}(s')$ approach each other from opposite sides of a corner, because of the discontinuity experienced by the normal vector $\hat{\mathbf{n}}$ when changing from one side to the other one. Choosing, e.g., for a polygonal billiard like those shown in Fig. 1 the boundary parametrization such that the corner with interior vertex angle θ_i is at \tilde{s}_i , and the two straight-line segments bordering it are symmetric with respect to the x axis, where the origin of the local coordinate system is chosen at \tilde{s}_i , then $\mathbf{r}(s) = [\tilde{s}_i - s](\cos\frac{\theta_i}{2}, \sin\frac{\theta_i}{2})$ for $\tilde{s}_{i-1} < s < \tilde{s}_i$ and $\mathbf{r}(s) = [s - \tilde{s}_i](\cos\frac{\theta_i}{2}, -\sin\frac{\theta_i}{2})$ for $\tilde{s}_i < s < \tilde{s}_{i+1}$. Since $\kappa(s)$ equals zero for both segments, $Q(s', s; k)$ vanishes when s and s' are along the same segment according to Eq. (A8), whereas for $\tilde{s}_{i-1} < s < \tilde{s}_i$ and $\tilde{s}_i < s' < \tilde{s}_{i+1}$ the prefactor is given by

$$\hat{\mathbf{n}}(s') \cdot \frac{\mathbf{r}(s') - \mathbf{r}(s)}{\rho(s', s)} = \frac{\epsilon \sin\theta_i}{\sqrt{\epsilon^2 + \epsilon'^2 - 2\epsilon\epsilon' \cos\theta_i}}, \quad (\text{A9})$$

with $\epsilon = \tilde{s}_i - s$ and $\epsilon' = s' - \tilde{s}_i$ which approaches $\cot(\theta_i/2)$ for $\epsilon \rightarrow \epsilon'$ and $\epsilon' \rightarrow 0$. Consequently, the Fredholm theory cannot be applied to prove that the matrix equation gives the correct eigenvalues with increasing n [20].

The shapes shown in Fig. 1 exhibit diffractive corners with angles $\theta_i = 3\pi/2$ for $i = 2, 7$ and $\theta_i = 3\pi/4$ for $i = 1, 5$ in (a). In Fig. 12 we show two examples of the eigenvectors solving Eq. (A5), that is, of the normal derivatives $u(s)$ along the boundary, where the positions of the corners are marked as in Fig. 1. The boundary functions exhibit cusps at the diffractive corners corresponding to the arc lengths $s = \tilde{s}_i$, $i = 1, 2, 5, 7$ and less pronounced ones at the $\pi/2$ corners at \tilde{s}_3 and \tilde{s}_4 . Yet, as clearly visible in Fig. 12 the curves for different values of b coincide, the only exception being the diffractive corners 2 and 7, where they exhibit sharp peaks of which the heights increase with decreasing distance of s from the respective corner, that is, with increasing b . A closer look at the cusps reveals that the boundary functions approach zero for the diffractive corners at \tilde{s}_1 or \tilde{s}_5 and increase algebraically \propto

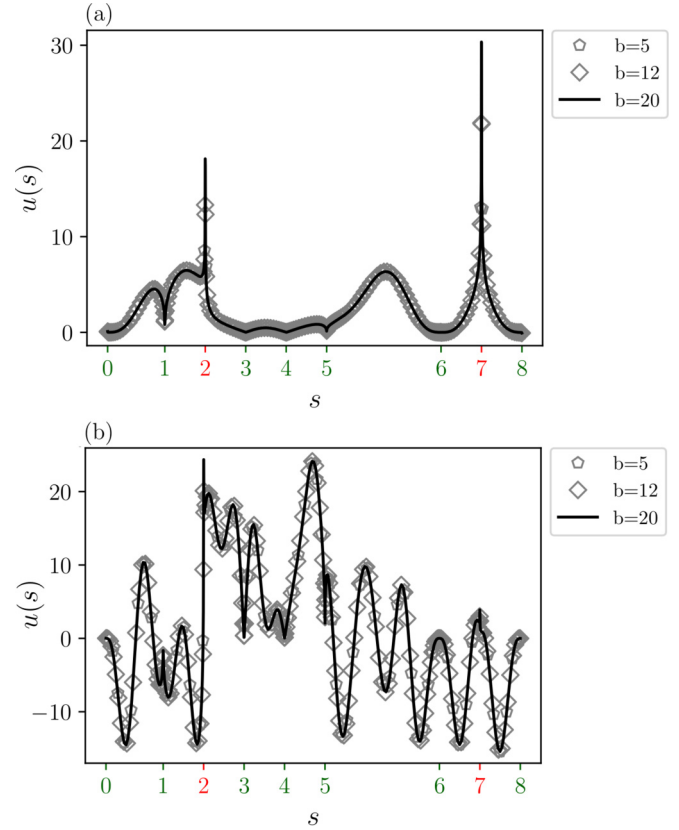


FIG. 12. Normal derivative of the wave functions along the boundary for the first (a) and the 19th (b) state of the QB with shape of domain 1 in Fig. 1 for different numbers b of quadrature points in a wavelength. The s values of the corners are marked using the same notation as in Fig. 1. The curves lie on top of each other, except at the diffractive corners marked by 2 and 7, where they exhibit sharp peaks of which the heights increase with decreasing distance of s from the corner, i.e., with increasing b .

$|s - \tilde{s}_i|^{-\delta}$ when approaching those at \tilde{s}_2 or \tilde{s}_7 from either side, where $0 \leq \delta < 1$. Actually, close to a corner with inner angle θ_i , the solution of the integral equation (A2) with Eq. (A9) approaches $u(s \rightarrow \tilde{s}_i) \simeq \frac{J_{\pi/\theta_i}(k|s-\tilde{s}_i|)}{|s-\tilde{s}_i|} \rightarrow |s - \tilde{s}_i|^{\pi/\theta_i - 1}$ [71] [see also Eq. (A1)] which is in accordance with our numerical results. Thus particular care has to be taken in the vicinity of the corners with $\theta_i = 3\pi/2$.

For boundaries with corners $\det[\mathcal{A}^{(N)}(k)]$ approaches zero for all values of k with increasing N [20,54]. It has been shown that, nevertheless, the zeros of the ratio $\det[\mathcal{A}^{(N)}(k)]/\det[\mathcal{A}^{(N)}(\epsilon)]$ with $\epsilon \ll k_1$ converge to the correct eigenvalues with increasing n thus justifying the use of the boundary integral method for their determination. This is illustrated in Fig. 13 for the first mode of domain 1 in Fig. 1 for $\epsilon = 0.02$ and a varying number b of quadrature points in a wavelength. Here, the discretization was chosen on each straight-line segment such that the value of the smallest distance of the s_i values from the corners decreases with increasing b . The curves are close to each other and the positions of their minima approach the same value $k^{(u)} = k_n^{(u)}$ with increasing b . Here, $k_n^{(u)}$ denotes the unfolded n th eigenvalue. Unfolding, i.e., the rescaling of the eigenvalues such that the

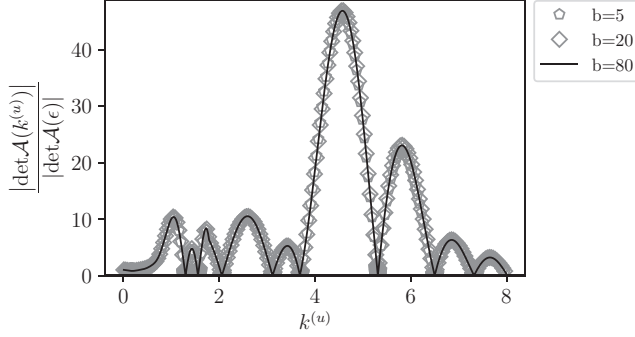


FIG. 13. Ratio $|\det[\mathcal{A}^{(N)}(k)]|/|\det[\mathcal{A}^{(N)}(\epsilon)]|$ versus the rescaled $k^{(u)}$ for domain 1 in Fig. 1 (see main text), with $\epsilon = 0.02$ for different numbers b of quadrature points in a wavelength.

spectral density is uniform, that is, independent of k and the mean spacing equals unity, was achieved with the Weyl formula for QBs providing the average integrated spectral density [72], $k_n^{(u)} = N^{\text{Weyl}}(k_n) = \frac{A}{4\pi} k_n^2 - \frac{L}{4\pi} k_n + \text{const}$, with A denoting the area of the billiard. The applicability of this regularization procedure to QBs with corners has been justified rigorously in Refs. [20,54]. Therefore, we used it to obtain the eigenvalues of the QBs considered in the present article.

APPENDIX B: COMPUTATION OF THE EIGENVALUES AND EIGENFUNCTIONS OF NBs

The eigenvalues and eigenfunctions are determined by solving a boundary integral equation for the two wave function components which is derived by proceeding similarly to the nonrelativistic case, with the free-space Green operator in coordinate representation being a 2×2 matrix [45],

$$-i\frac{k}{4} \oint_{\partial\Omega} ds \psi_1^*(s) \{H_0^{(1)}[k\rho(s, s')]\} - e^{-i\alpha(s)} e^{i\xi(s, s')} H_1^{(1)}[k\rho(s, s')] = \frac{\chi}{2} \psi_1^*(s'), \quad (\text{B1})$$

$$i\frac{k}{4} \oint_{\partial\Omega} ds \psi_2^*(s) \{H_0^{(1)}[k\rho(s, s')]\} + e^{i\alpha(s)} e^{-i\xi(s, s')} H_1^{(1)}[k\rho(s, s')] = \frac{\chi}{2} \psi_2^*(s'), \quad (\text{B2})$$

where

$$e^{i\xi(s, s')} = \frac{z(s) - z(s')}{|z(s) - z(s')|}, \quad \rho(s, s') = |z(s) - z(s')|. \quad (\text{B3})$$

We determined the value of χ by proceeding as in [69] yielding the result given in Eq. (A3). For both equations the integrand has a singularity for $s \rightarrow s'$, which can be removed by combining them and applying again the boundary condition Eq. (5) yielding

$$\frac{ik}{4} \oint_{\partial\Omega} ds \tilde{Q}(s', s; k) \psi_1^*(s) = \chi \psi_1^*(s'), \quad (\text{B4})$$

with

$$\begin{aligned} \tilde{Q}(s', s; k) = & [e^{i[\alpha(s') - \alpha(s)]} - 1] H_0^{(1)}[k\rho(s, s')] \\ & + [e^{i\alpha(s') - i\xi(s, s')} + e^{-i\alpha(s) + i\xi(s, s')}] H_1^{(1)}[k\rho(s, s')]. \end{aligned} \quad (\text{B5})$$

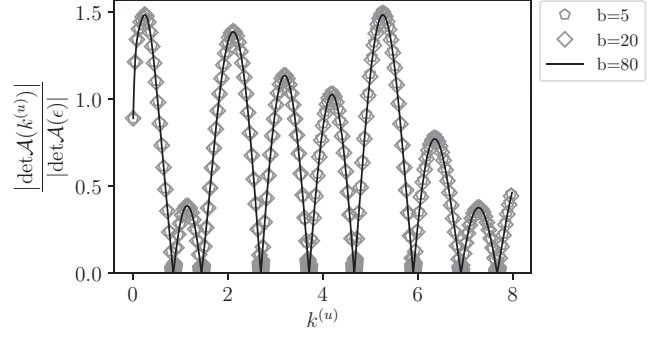


FIG. 14. Same as Fig. 13 for the corresponding NB.

The corresponding boundary integral equation for $\psi_2^*(s)$ is deduced from Eq. (B4) by applying Eq. (5). Equation (B4) is transformed to a matrix equation by proceeding as described in Appendix A and discretizing the boundary parameter s using Gauss-Legendre quadrature,

$$\det[\mathcal{A}^{(N)}(k)] = 0, \quad \mathcal{A}_{ij}^{(N)}(k) = \delta_{ij} - \tilde{Q}^{(N)}(s_i, s_j; k) w_j. \quad (\text{B6})$$

Actually, to improve the precision of the eigenvalues we used the expanded boundary integral method which we developed in Ref. [53]. Like in the nonrelativistic case, the zeros of this equation are found by plotting the absolute value of either $\det[\mathcal{A}^{(N)}(k)]$ or of the eigenvalue $e_{\min}(k)$ of $\mathcal{A}^{(N)}(k)$, which is closest to zero versus k , and determining the positions of the minima, which yield the discrete solutions k_n of Eq. (B6) up to a numerical error. An estimate of the latter is provided by their deviations from zero. Similarly, it can be shown that these solutions converge with increasing N to those of the boundary integral equation (B4) for billiards with a smooth boundary. In fact, in distinction to the nonrelativistic case, the integrand of Eq. (B4) vanishes when $s' \rightarrow s$, since the prefactors of $H_0^{(1)}[k\rho(s, s')]$ and $H_1^{(1)}[k\rho(s, s')]$ approach zero faster than their singularities diverge for $\rho(s, s') \rightarrow 0$ [53]. Yet, as in the nonrelativistic case, the singularities cannot be compensated by the respective prefactor when $z(s)$ and $z(s')$ approach each other from opposite sides of a corner, because $\alpha(s' \rightarrow s)$ experiences a jump at the corner. Using the same notation as for Eq. (A9), $\tilde{Q}(s', s; k)$ equals zero when both s and s' are chosen along the same side, whereas when s and s' are on opposite sides, i.e., $\tilde{s}_{i-1} < s < \tilde{s}_i$ and $\tilde{s}_i < s' < \tilde{s}_{i+1}$, the prefactor of $H_0^{(1)}[k\rho(s, s')]$ equals $-(1 + e^{-i\theta_i})$ and that of $H_1^{(1)}[k\rho(s, s')]$ equals

$$\begin{aligned} & [e^{i\alpha(s') - i\xi(s, s')} + e^{-i\alpha(s) + i\xi(s, s')}] \\ & = -i(1 + e^{-i\theta_i}) \frac{(\epsilon - \epsilon')}{\sqrt{\epsilon^2 + \epsilon'^2 - 2\epsilon\epsilon' \cos \theta_i}}, \end{aligned} \quad (\text{B7})$$

with $\epsilon = \tilde{s}_i - s$ and $\epsilon' = s' - \tilde{s}_i$, which in contrast to the prefactor in Eq. (A9) approaches zero for $\epsilon \rightarrow \epsilon'$ and $\epsilon' \rightarrow 0$, yet not sufficiently fast to compensate the $1/\rho$ singularity of $H_1^{(1)}[k\rho(s, s')]$.

Figure 14 shows the ratio $|\det[\mathcal{A}^{(N)}(k)]|/|\det[\mathcal{A}^{(N)}(\epsilon = 0.02)]|$ for the NB with the shape of domain 1 in Fig. 1 for different numbers b of quadrature points versus the unfolded $k^{(u)}$. Unfolding was performed with the Weyl formula for NBs [45], $k_n^{(u)} = N^{\text{Weyl}}(k_n) = \frac{A}{4\pi} k_n^2 + \text{const}$, where the perimeter

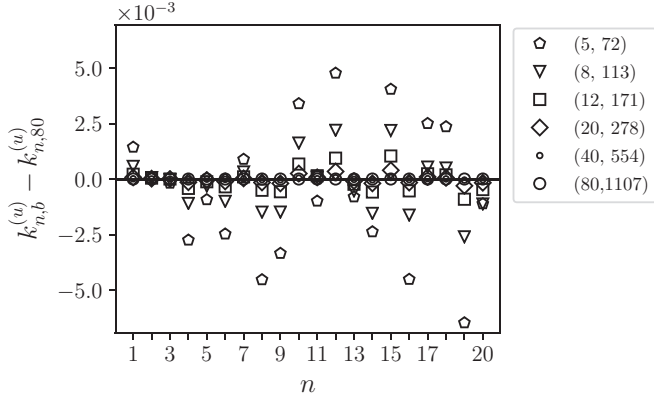


FIG. 15. Illustration of the convergence of the solutions k_n of the boundary integral equation (B4) with increasing number N of quadrature points for the NB with the shape of domain 1 in Fig. 1. Shown is the difference between the unfolded eigenvalues $k_{n,b}^{(u)}$ and $k_{n,80}^{(u)}$ with $b \leq 80$ denoting the number of quadrature points in a wavelength for the 20th eigenvalue. From light color to dark (b, N) = (5, 72), (8, 114), (12, 170), (15, 212), (20, 278), (40, 555), and (80, 1107).

term $\frac{\mathcal{L}}{4\pi} k_n$ occurring in that for the corresponding QB [72] is absent. The different curves coincide and the positions of their minima converge to the same values $k = k_n$ with increasing b . This is demonstrated for the first 20 eigenstates in Fig. 15, which shows the deviations of the unfolded eigenvalues $k_{n,b}^{(u)}$, with $b = 5, 8, 12, 15, 20, 40, 80$ denoting the number of quadrature points fitting into a wavelength, from those obtained for the largest considered $b = 80$. In Fig. 16 we show two examples of the eigenvectors solving Eq. (B6), that is, of the wave function component $\psi_1(s)$ along the boundary for three values of the number of quadrature points b in a wavelength. The positions of the corners are marked as in Fig. 1. The boundary functions exhibit, like in the nonrelativistic case, cusps at all corners of domain 1 except at the $\pi/4$ corners at \tilde{s}_0, \tilde{s}_6 and are especially pronounced at the diffractive corners \tilde{s}_2 and \tilde{s}_7 , where they have sharp peaks. The boundary wave functions for different values of b differ only there. When approaching a diffractive corner at \tilde{s}_i , $i = 2, 7$ (see Fig. 1) from either side, the boundary functions again increase algebraically $\propto |s - \tilde{s}_i|^{-\delta}$, but the value of δ is smaller than in the nonrelativistic case. Consequently, the drawbacks of the boundary integral equation due to the presence of singularities cause less problems in the numerical analysis of NBs than they do in QBs. Yet, as outlined in Appendix A, the boundary integral method including the regularization procedure yields the correct eigenvalues for the latter. Thus we may expect that the same holds for NBs. We, indeed, were able to compute the first 1000 eigenvalues with high accuracy with the expanded boundary integral method [53], as demonstrated in Fig. 17. There the absolute value of the smallest eigenvalue of $\mathcal{A}(k_n)$ is plotted versus n , which is supposed to equal zero at the eigenvalues $k = k_n$ solving the boundary integral equation (B4). It takes values of the order 10^{-4} or less. Actually, according to our experience this accuracy is sufficient to obtain the eigenvalues of NBs with a smooth boundary with a high precision.

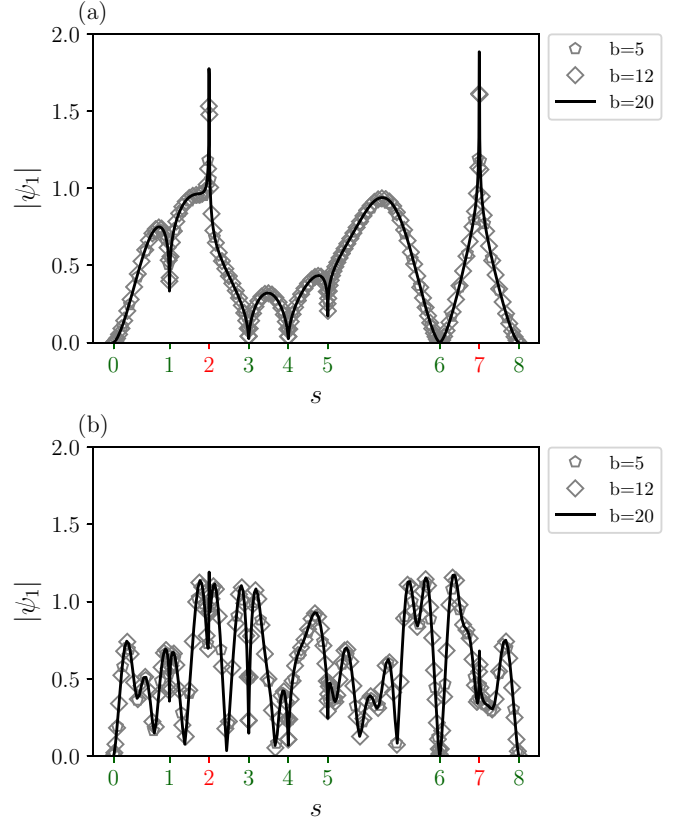


FIG. 16. Same as Fig. 12 for the modulus of the first wave function component $\psi_1(s)$ along the boundary.

APPENDIX C: ABSENCE OF NODAL LINES IN NBs

To demonstrate that the real and imaginary parts of the wave function components have nodal lines at distinct locations let us assume that $\psi_1(\mathbf{r})$ has a nodal line denoted by $\tilde{\Gamma}$, that is, that its real and imaginary parts vanish simultaneously

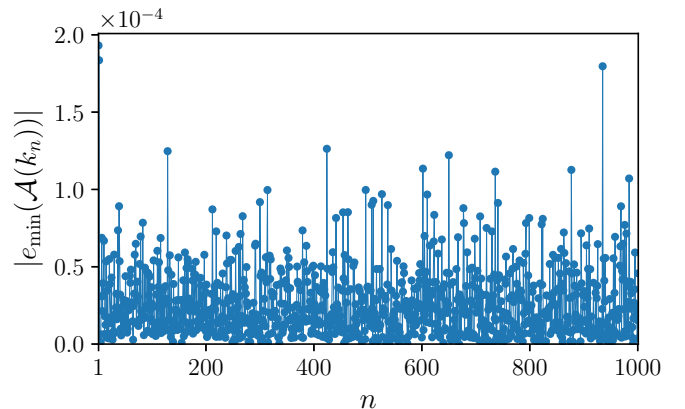


FIG. 17. Absolute value of the smallest eigenvalues $e_{\min}(k_n)$ of the matrix $\mathcal{A}(k_n)$ defined in Eq. (B6) at the minima of $|\det[\mathcal{A}(k)]|$ corresponding—within the numerical error—to solutions $k = k_n$ of Eq. (B6) for a NB of the shape of domain 1 in Fig. 1(a). Their deviations from zero provide an estimate for the accuracy of the numerical evaluation of Eqs. (B4) and (B6). The number of quadrature points equaled $b = 80$.

along that curve, and choose perpendicular coordinates (t, n) with t varying along $\tilde{\Gamma}$ and n normal to it. Denoting the tangential vector to $\tilde{\Gamma}$ by $\mathbf{t} = [-\sin \beta(t), \cos \beta(t)]$ and the normal one by $\mathbf{n} = [\cos \beta(t), \sin \beta(t)]$ with $\beta(t)$ corresponding to the angle between \mathbf{n} and the x axis, and using $\partial_t = \mathbf{t} \cdot \nabla$ and $\partial_n = \mathbf{n} \cdot \nabla$, yields

$$\partial_x \pm i\partial_y = e^{\pm i\beta(t)}(\partial_n \pm i\partial_t). \quad (\text{C1})$$

Since $\psi_1(\mathbf{r})|_{\tilde{\Gamma}} = 0$ is constant along $\tilde{\Gamma}$, we have $\partial_t \psi_1(\mathbf{r})|_{\tilde{\Gamma}} = 0$. Transforming the Dirac Hamiltonian from Cartesian to (t, n) coordinates and using these properties, Eq. (4) becomes

$$\begin{aligned} k\psi_2(\mathbf{r})|_{\tilde{\Gamma}} &= -i e^{i\beta(t)} \partial_n \psi_1(\mathbf{r})|_{\tilde{\Gamma}}, \\ 0 &= (\partial_n - i\partial_t)\psi_2(\mathbf{r})|_{\tilde{\Gamma}}. \end{aligned} \quad (\text{C2})$$

From these equations we may immediately deduce that ψ_1 and ψ_2 cannot exhibit nodal lines simultaneously, since this would imply that $\partial_t \psi_j(\mathbf{r})|_{\tilde{\Gamma}} = 0$ and $\partial_n \psi_j(\mathbf{r})|_{\tilde{\Gamma}} = 0$ for $j =$

1, 2. Hence, in this case, both wave function components vanish not only along a line, but in some region of the billiard area.

The second condition on the partial derivatives of ψ_2 implies that it can only depend on $\tilde{z} = n + it$. Applying the Dirac Hamiltonian in Eq. (4) twice to ψ yields with Eq. (C2)

$$\left(\frac{\partial^2}{\partial n^2} + \frac{\partial^2}{\partial t^2} + \dot{\beta}(t)\frac{\partial}{\partial n}\right)\psi_1(\mathbf{r})|_{\tilde{\Gamma}} = 0, \quad (\text{C3})$$

$$\left(\frac{\partial^2}{\partial n^2} + \frac{\partial^2}{\partial t^2}\right)\psi_2(\mathbf{r})|_{\tilde{\Gamma}} = -k^2\psi_2(\mathbf{r})|_{\tilde{\Gamma}}. \quad (\text{C4})$$

Summarizing, ψ_1 can only have a nodal line when the normal derivatives of ψ_2 are related according to the second of Eqs. (C2), and ψ_2 itself is governed by the Schrödinger equation (C4) along $\tilde{\Gamma}$ with the first of these equations and Eq. (5) as conditions along $\tilde{\Gamma}$ and the billiard boundary, respectively, which, typically, is not the case.

-
- [1] M. Kac, *Am. Math. Mon.* **73**, 1 (1966).
[2] O. Giraud and K. Thas, *Rev. Mod. Phys.* **82**, 2213 (2010).
[3] H.-J. Stöckmann, *Quantum Chaos: An Introduction* (Cambridge University Press, Cambridge, UK, 2000).
[4] B. Dietz and A. Richter, *Chaos* **25**, 097601 (2015).
[5] M. Levitin, L. Parnowski, and I. Polterovich, *J. Phys. A* **39**, 2073 (2006).
[6] D. Jakobson, M. Levitin, N. Nadirashvili, and I. Polterovich, *J. Comput. Appl. Math.* **194**, 141 (2006), special issue: 60th birthday of Prof. Brian Davies.
[7] R. Melrose, Math. Sci. Res. Inst. Rep. No. 048-83 (1983) (unpublished).
[8] B. Osgood, R. Phillips, and P. Sarnak, *J. Funct. Anal.* **80**, 212 (1988).
[9] T. Sunada, *Ann. Math.* **121**, 169 (1985).
[10] C. Gordon, D. L. Webb, and S. Wolpert, *B. Am. Math. Soc.* **27**, 134 (1992).
[11] P. Bérard, *Math. Ann.* **292**, 547 (1992).
[12] C. Gordon, D. Webb, and S. Wolpert, *Invent. Math.* **110**, 1 (1992).
[13] S. Sridhar and A. Kudrolli, *Phys. Rev. Lett.* **72**, 2175 (1994).
[14] C. Gordon and D. Webb, *Proc. Am. Math. Soc.* **120**, 981 (1994).
[15] S. J. Chapman, *Am. Math. Mon.* **102**, 124 (1995).
[16] P. Buser, J. Conway, P. Doyle, and K.-D. Semmler, *Internat. Math. Res. Notices* **1994**, 391 (1994).
[17] A. Dhar, D. M. Rao, Udaya Shankar N., and S. Sridhar, *Phys. Rev. E* **68**, 026208 (2003).
[18] B. D. Sleeman and H. Chen, *Rev. Mat. Iberoam.* **16**, 351 (2000).
[19] S. Tasaki, T. Harayama, and A. Shudo, *Phys. Rev. E* **56**, R13 (1997).
[20] Y. Okada, A. Shudo, S. Tasaki, and T. Harayama, *J. Phys. A: Math. Gen.* **38**, L163 (2005).
[21] R. Band, O. Parzanchevski, and G. Ben-Shach, *J. Phys. A* **42**, 175202 (2009).
[22] O. Parzanchevski and R. Band, *J. Geom. Anal.* **20**, 439 (2010).
[23] B. Gutkin and U. Smilansky, *J. Phys. A* **34**, 6061 (2001).
[24] R. Band, A. Sawicki, and U. Smilansky, *J. Phys. A* **43**, 415201 (2010).
[25] R. Band, A. Sawicki, and U. Smilansky, *Acta Phys. Pol. A* **120**, 149 (2011).
[26] O. Hul, M. Ławniczak, S. Bauch, A. Sawicki, M. Kuś, and L. Sirko, *Phys. Rev. Lett.* **109**, 040402 (2012).
[27] P. G. Silvestrov and K. B. Efetov, *Phys. Rev. Lett.* **98**, 016802 (2007).
[28] L. A. Ponomarenko, F. Schedin, M. I. Katsnelson, R. Yang, E. W. Hill, K. S. Novoselov, and A. K. Geim, *Science* **320**, 356 (2008).
[29] F. Libisch, C. Stampfer, and J. Burgdörfer, *Phys. Rev. B* **79**, 115423 (2009).
[30] J. Wurm, A. Rycerz, Í. Adagideli, M. Wimmer, K. Richter, and H. U. Baranger, *Phys. Rev. Lett.* **102**, 056806 (2009).
[31] L. Huang, Y.-C. Lai, D. K. Ferry, S. M. Goodnick, and R. Akis, *Phys. Rev. Lett.* **103**, 054101 (2009).
[32] L. Huang, Y.-C. Lai, and C. Grebogi, *Phys. Rev. E* **81**, 055203(R) (2010).
[33] J. Wurm, K. Richter, and Í. Adagideli, *Phys. Rev. B* **84**, 075468 (2011).
[34] A. Rycerz, *Phys. Rev. B* **85**, 245424 (2012).
[35] A. Rycerz, *Phys. Rev. B* **87**, 195431 (2013).
[36] M. Polini, F. Guinea, M. Lewenstein, H. C. Manoharan, and V. Pellegrini, *Nat. Nanotechnol.* **8**, 625 (2013).
[37] B. Dietz, T. Klaus, M. Miski-Oglu, and A. Richter, *Phys. Rev. B* **91**, 035411 (2015).
[38] B. Dietz, T. Klaus, M. Miski-Oglu, A. Richter, M. Wunderle, and C. Bouazza, *Phys. Rev. Lett.* **116**, 023901 (2016).
[39] K. S. Novoselov, A. K. Geim, S. V. Morozov, D. Jiang, Y. Zhang, S. V. Dubonos, I. V. Grigorieva, and A. A. Firsov, *Science* **306**, 666 (2004).
[40] C. W. J. Beenakker, *Rev. Mod. Phys.* **80**, 1337 (2008).
[41] A. H. Castro Neto, F. Guinea, N. M. R. Peres, K. S. Novoselov, and A. K. Geim, *Rev. Mod. Phys.* **81**, 109 (2009).
[42] Y.-C. Lai, H.-Y. Xu, L. Huang, and C. Grebogi, *Chaos* **28**, 052101 (2018).
[43] L. Huang, H.-Y. Xu, C. Grebogi, and Y.-C. Lai, *Phys. Rep.* **753**, 1 (2018).

- [44] B. Dietz and A. Richter, *Phys. Scr.* **94**, 014002 (2019).
- [45] M. V. Berry and R. J. Mondragon, *Proc. R. Soc. London A* **412**, 53 (1987).
- [46] O. Giraud, *J. Phys. A* **37**, 2751 (2004).
- [47] M. L. Mehta, *Random Matrices* (Academic Press, London, 1990).
- [48] M. V. Berry, *Philos. Trans. R. Soc. London A* **287**, 237 (1977).
- [49] G. Casati, F. Valz-Gris, and I. Guarnieri, *Lett. Nuovo Cimento* **28**, 279 (1980).
- [50] O. Bohigas, M. J. Giannoni, and C. Schmit, *Phys. Rev. Lett.* **52**, 1 (1984).
- [51] M. V. Berry and M. Tabor, *J. Phys. A* **10**, 371 (1977).
- [52] P. J. Richens and M. V. Berry, *Physica D* **2**, 495 (1981).
- [53] P. Yu, B. Dietz, and L. Huang, *New J. Phys.* **21**, 073039 (2019).
- [54] Y. Okada, A. Shudo, S. Tasaki, and T. Harayama, *J. Phys. A: Math. Gen.* **38**, 6675 (2005).
- [55] M. V. Berry and M. Wilkinson, *Proc. R. Soc. London A* **392**, 15 (1984).
- [56] M. V. Berry and M. Wilkinson, *Proc. R. Soc. London A* **459**, 1261 (2003).
- [57] H. Wu, D. W. L. Sprung, and J. Martorell, *Phys. Rev. E* **51**, 703 (1995).
- [58] N. Rosenzweig and C. Porter, *Phys. Rev.* **120**, 1698 (1960).
- [59] G. Lenz and F. Haake, *Phys. Rev. Lett.* **67**, 1 (1991).
- [60] V. K. B. Kota, *Embedded Random Matrix Ensembles in Quantum Physics* (Springer-Verlag, Heidelberg, 2014).
- [61] M. Sieber, U. Smilansky, S. C. Creagh, and R. G. Littlejohn, *J. Phys. A* **26**, 6217 (1993).
- [62] P. Yu, Z.-Y. Li, H.-Y. Xu, L. Huang, B. Dietz, C. Grebogi, and Y.-C. Lai, *Phys. Rev. E* **94**, 062214 (2016).
- [63] W. A. Gaddah, *J. Phys. A* **51**, 385304 (2018).
- [64] L. Fox, P. Henrici, and C. Moler, *SIAM J. Numer. Anal.* **4**, 89 (1967).
- [65] A. H. Barnett and C. T. Betcke, *Chaos* **17**, 043125 (2007).
- [66] T. Betcke, *SIAM J. Sci. Comput.* **30**, 1278 (2008).
- [67] T. A. Driscoll, *SIAM Rev.* **39**, 1 (1997).
- [68] J. Descloux and M. Tolley, *Comput. Methods Appl. Mech. Eng.* **39**, 37 (1983).
- [69] I. Kosztin and K. Schulten, *Int. J. Mod. Phys. C* **8**, 293 (1997).
- [70] A. Bäcker, *Numerical Aspects of Eigenvalue and Eigenfunction Computations for Chaotic Quantum Systems* (Springer, Berlin, 2003), pp. 91–144.
- [71] K. Serkh and V. Rokhlin, *Proc. National Acad. Sci.* **113**, 9171 (2016).
- [72] H. P. Baltes and E. R. Hilf, *Spectra of Finite Systems* (Bibliographisches Institut, Mannheim, 1976).